Macromolecules
COMMUNICATION TO THE EDITOR

Macromolecules **2010**, *43*, 4449–4452 **4449**
DOI: 10.1021/ma100510p

Inverted Phases Induced by Chain Architecture in ABAC Tetrablock Terpolymers

Michael J. Bluemle,[†] Jingwen Zhang,[†] Timothy P. Lodge,[†,‡] and Frank S. Bates*[,†]

[†]*Department of Chemical Engineering and Materials Science and* [‡]*Department of Chemistry, University of Minnesota, Minneapolis, Minnesota 55455*

Received March 5, 2010
Revised Manuscript Received April 22, 2010

Self-assembly of block polymer melts into periodically ordered microstructures has proved attractive for generating materials with strict control over length scale and morphology.[1] The simplest class of linear block polymers, AB diblocks, generate only four stable phases. (Takenaka and co-workers[2] recently reported a fifth morphology, an orthorhombic network phase (O^{70}) with *Fddd* symmetry, in a poly(styrene-*b*-isoprene) diblock copolymer over a narrow slice of parameter space). At strong or intermediate segregation strength ($\chi_{AB}N \gg 10$, where χ_{AB} is the segment−segment interaction parameter and N is the overall degree of polymerization), these morphologies are dictated solely by the block volume fractions (f). Highly asymmetric diblocks ($f \sim 0.1-0.15$) produce spherical domains of the minority blocks, arranged with BCC order in a matrix of the majority blocks. Hexagonally packed cylinders occur when the molecular asymmetry decreases ($f \sim 0.15-0.3$), while alternating lamellae of A-rich and B-rich domains are most stable when the volume fractions of the blocks are comparable ($f \sim 0.35-0.5$). These "classical" phases are complemented by the bicontinuous double gyroid, which occurs over a narrow region of composition space between cylinders and lamellae ($f \sim 0.3-0.35$). While block conformational asymmetry[3] and modest polydispersity[4] can shift these morphology boundaries, the overall topology of the AB diblock phase portrait remains unchanged.

The number and geometrical complexity of morphologies increases dramatically with the addition of a third dissimilar block, as in ABC triblocks. The number of possible block interfaces (A/B, A/C, and B/C) triples, which complicates the free energy balance that determines self-assembly behavior. At this time, over 30 ordered morphologies have been reported for linear triblock terpolymers.[5−16] Among the ABC triblock microstructures are core−shell analogues of the sphere, cylinder, and double gyroid phases found in AB diblocks.[9,12,17] The core−shell cylindrical and gyroid phases are particularly attractive candidates for the creation of mechanically robust solid-state electrolytes, nanoporous templates, and semipermeable membranes.

We are especially interested in using molecular architecture to produce new ordered morphologies, or to expand the range of block compositions that lead to a given microstructure. This has led us to explore the self-assembly behavior of ABAC tetrablock terpolymers. In a previous study, we reported an unanticipated network structure in a series of poly(cyclohexylethylene-*b*-ethylene-*b*-cyclohexylethylene-*b*-dimethylsiloxane) tetrablocks.[18] In this communication we describe the bulk morphological behavior of a sequence of poly(styrene-*b*-isoprene-*b*-styrene-*b*-ethylene oxide) SISO terpolymers with $f_S \cong f_I$ and f_O between 0 and 30% (the S is divided equally between the two S blocks, see Scheme 1).

*Corresponding author.

Scheme 1. Molecular Structure of SISO Tetrablock Terpolymers

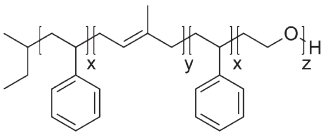

Incorporation of O into a block polymer is appealing for two reasons: the growth of O can be initiated from a hydroxyl-terminated macromolecule,[19] and O containing block polymers have received widespread attention as electrolytes.[20] Additionally, SISO represents a variation of the well-studied ISO system,[14,16,21] making it ideal for examining differences in phase behavior that arise from chain architecture alone.

Nine SISO tetrablocks were generated by the reinitiation and polymerization of ethylene oxide from a single batch of hydroxyl-terminated SIS copolymer, using a previously published multistep approach.[13,19] This method ensures that the only variation within the series of SISO terpolymers is the O block length (parameter z in Scheme 1). The molecular characteristics of the parent SIS and SISO terpolymers are summarized in Table 1. Molecular weights (M_n and M_w) and polydispersities (M_w/M_n) were determined by size exclusion chromatography. The block volume fractions (f_S, f_I, f_O) were obtained by ^{1}H NMR and are referenced to published homopolymer densities at 140 °C.[22] 0.5 wt % of BHT antioxidant was added to the block polymers prior to structural characterization. Morphological assignments were made by utilizing a combination of small-angle X-ray scattering (SAXS), dynamic mechanical spectroscopy (DMS), and transmission electron microscopy (TEM).

Two-dimensional synchrotron SAXS data were collected at the Advanced Photon Source at Argonne National Laboratory using an experimental setup described elsewhere.[16] The diffraction data were azimuthally averaged and are presented as intensity as a function of scattering wave vector $|\boldsymbol{q}| = q = 4\pi\lambda^{-1}\sin(\theta/2)$, where λ is the radiation wavelength and θ is the scattering angle. Samples were annealed above the order−disorder transition temperature (T_{ODT}) for 5 min, or at 250 °C for samples with $T_{ODT} > 250$ °C. SAXS powder patterns from the SIS triblock and nine SISO tetrablocks are presented in Figure 1. The SAXS data for SIS and SISO-1 (both collected at 80 °C) show only a single, broad peak, which we associate with the disordered state. Increasing the O content to $0.07 \le f_O \le 0.09$ (specimens SISO-2 (140 °C), SISO-3 (80 °C), and SISO-4 (140 °C)) leads to qualitatively different scattering behavior; an additional maximum at higher q is apparent, but the principal peak remains broad, implying limited long-range structural order. We attribute these results to liquid-like packed (LLP) spheres,[23−30] which were corroborated by TEM and DMS measurements (see below). If we assign the broad bump at $q \cong 0.058$ Å^{-1} (Figure 1, SISO-2) as the first maximum in the spherical form factor,[23] we obtain a sphere radius of 99 Å. Taking the primary peak as the (110) reflection of a BCC lattice yields a core volume fraction of 0.53, which is equivalent to $f_S + f_O$ and suggests that the spheres consist of both S and O. The SAXS patterns produced by SISO tetrablocks with $f_O \ge 0.12$ (SISO-4, −5, −6, −7, −8, and −9 collected at 140 °C) are strikingly different than the other samples, each containing at least three well-defined scattering peaks. The scattering pattern for SISO-9 displays peaks at $q/q^* = \sqrt{1}, \sqrt{3}, \sqrt{4}, \sqrt{7}$, and $\sqrt{9}$, where q^* is the principal peak location, consistent with hexagonal (HEX) symmetry. Characteristic structural

Published on Web 04/28/2010

Table 1. Characterization Data for SIS Triblock and SISO Tetrablock Terpolymers

polymer	M_n, kDa	M_w/M_n	f_S[a]	f_I[a]	f_O[a]	X_c, O[b]	phase[c]	T_{ODT}, °C[d]	d, nm[e]
SIS	20.8	1.03	0.51	0.49	0	–	DIS	< 80	13.4 (80)
SISO-1	21.7	1.04	0.48	0.48	0.04	0	DIS	< 80	15.4 (80)
SISO-2	22.7	1.07	0.46	0.47	0.07	30	LLP spheres	174	17.6
SISO-3	23.0	1.04	0.46	0.46	0.08	37	LLP spheres	196	18.7 (80)
SISO-4	23.2	1.07	0.45	0.46	0.09	41	LLP spheres	225	18.9
SISO-5	24.2	1.04	0.44	0.44	0.12	50	HEX	> 250	21.0
SISO-6	24.6	1.10	0.43	0.43	0.14	54	HEX	> 250	20.0
SISO-7	25.3	1.04	0.42	0.42	0.16	55	HEX	> 250	20.9
SISO-8	26.4	1.12	0.40	0.41	0.19	53	HEX	> 250	22.2
SISO-9	31.1	1.12	0.35	0.35	0.30	64	HEX	> 250	28.1

[a] Volume fractions were calculated from published melt density data at 140 °C.[22] [b] Fraction of crystallinity in the O domains as measured by DSC. [c] DIS: disordered. LLP spheres: liquid-like packing of spheres. Hex: hexagonally packed cylinders. [d] Order−disorder transition temperatures determined by DMS. [e] Characteristic morphological length scale ($d = 2\pi/q^*$) at 140 °C unless noted in parentheses.

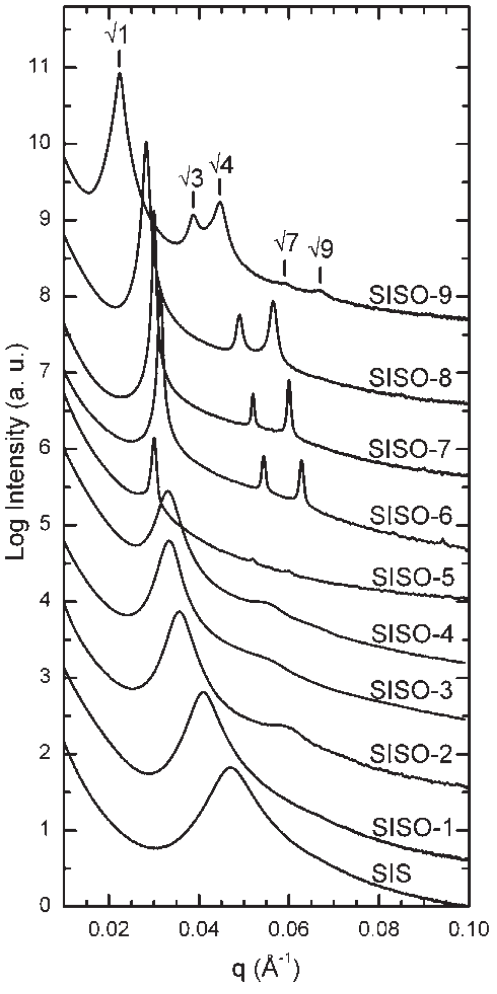

Figure 1. Synchrotron SAXS patterns obtained from SIS triblock and SISO tetrablock samples. Data were collected at 80 °C (SIS, SISO-1, and -3) or 140 °C (SISO-2, -4, -5, -6, -8, and -9). The broad primary peak and lack of higher order reflections for SIS and SISO-1 are consistent with a disordered melt. The patterns for SISO-2, -3, and -4 do not exhibit long-range structural order, but display a bump at higher q attributed to a maximum in the spherical form factor. The Bragg reflections for SISO-5, -6, -7, -8, and -9 are consistent with hexagonal symmetry, which have been indexed for SISO-9.

length scales $d = 2\pi/q^*$ for the disordered, LLP spheres, and HEX samples are summarized in Table 1.

TEM was utilized to characterize the morphologies of the LLP sphere and HEX phases identified by SAXS. TEM micrographs of selected SISO samples were obtained using a JEOL 1210 microscope operating at 120 kV. Specimens were annealed at elevated temperatures (150 and 170 °C for SISO-2 and SISO-6,

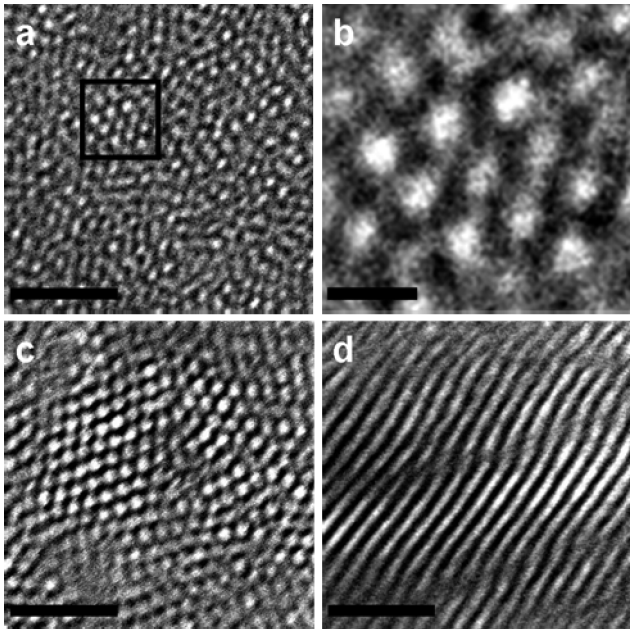

Figure 2. TEM micrographs generated from (a, b) SISO-2 ($f_O = 0.07$) and (c, d) SISO-6 ($f_O = 0.14$). The dark regions result from selective staining of the I domains with OsO_4. (a) I domains are microphase-separated from lighter S and O domains, but long-range order is lacking in the specimen. (b) Magnified view of the area marked with a square in part a, displaying short-range periodic order. (c) Hexagonal packing of unstained S and O domains within the I matrix is readily apparent. (d) Orthogonal view displaying the long axis of cylinders. The scale bars denote 100 nm except for 20 nm in part b.

respectively) for 3 days prior to quenching into liquid nitrogen to preserve the melt morphology. Thin slices (~70 nm) of polymer were prepared by cryo-microtoming at −70 °C and collected on copper grids. Contrast was attained by exposing the polymer slices to the vapor from a 4% aqueous solution of osmium tetroxide for 10 min. The heavy metal oxide reacts preferentially with the I domains providing electron mass density contrast within these materials. The images in Figure 2, parts a and b were generated from SISO-2. Light circular regions associated with S and O appear to be dispersed without long ranged order in a dark matrix of I. However, careful examination reveals restricted regions of short ranged microdomain periodicity (Figure 2b). These TEM results are consistent with our interpretation of the SAXS results (Figure 1) as a spherical microstructure lacking long-range order. Micrographs recorded from SISO-6 are consistent with the HEX symmetry identified by SAXS (Figure 2c) and allow assignment of a cylindrical phase (Figure 2d). Like SISO-2, regions of S and O are arranged within the continuous I matrix, but are hexagonally packed and display areas of long-range

order in accordance with the relatively narrow diffraction peaks found in Figure 1. The TEM results provide definitive evidence of inverted phases with the majority constituents (S and O) forming spheres and cylinders.

Two types of DMS experiments were conducted between 80 and 250 °C, well above the glass transition (T_g) and melting temperatures (T_m) of the S ($T_g \cong 60$ °C) and O ($T_m < 60$ °C) blocks. Isochronal ($\omega = 1$ rad/s) measurements of the elastic (G') and loss (G'') moduli at a constant heating rate of 2 °C/min yielded the T_{ODT} values listed in Table 1; no order−order transitions (discontinuities in G' or G'' prior to T_{ODT}) were recorded during these experiments. G' and G'' were also monitored during isothermal frequency scans ($0.1 \leq \omega \leq 100$ rad/s) to characterize the linear viscoelastic properties of the polymers. Figure 3 displays the frequency-dependent rheological properties from three SISO tetrablocks, representative of the three phases identified on the basis of SAXS and TEM. These plots were constructed using time−temperature superposition (TTS) of tan δ, where tan $\delta = G''/G'$, with a reference temperature (T_{ref}) of 80 °C. (While TTS is not valid fundamentally for such rheologically complex materials it does facilitate comparison of data obtained at different temperatures). SISO-1 ($f_O = 0.04$, upper panel in Figure 3) displays terminal linear viscoelastic behavior ($G' \sim \omega$ and $G'' \sim \omega^2$) over the investigated temperature range consistent with the disordered state and the SAXS results (Figure 1). The isothermal frequency results generated from SISO-4 ($f_O = 0.09$, middle panel in Figure 3) are vastly different in appearance and are consistent with an ordered microstructure. The low frequency plateau in G' has been attributed to triply periodic morphologies[31] such as the three-dimensional sphere phase identified in this sample with SAXS and TEM. We associate the viscoelastic response of decreasing G' and G'' with decreasing ω (SISO-8, $f_O = 0.19$, bottom panel in Figure 3) to the HEX cylinder phase assigned by SAXS for SISO-5, −6, −7, −8, and −9.

On the basis of SAXS, TEM, and DMS characterization results, the sequence of phases associated with this series of SISO tetrablock terpolymers can be summarized as disordered to spheres with short-range order (liquid-like packing) to hexagonally packed cylinders with increasing f_O. A lack of long-range microstructural order in SISO-2, SISO-3, and SISO-4 ($0.07 \leq f_O \leq 0.09$) may reflect slow equilibration kinetics likely exacerbated by the SISO chain architecture. Cavicchi and Lodge proposed that the development of well-ordered BCC arrays in sphere-forming block polymers is hindered by the expulsion and reinsertion of chains from one sphere to another during domain equilibration,[32] a restriction that will be amplified by the tetrablock architecture. Additional high-temperature annealing of these samples may yield microstructures with long-range, periodic order. While we can not visualize microphase separation of the O and S blocks with our TEM staining method, DSC experiments suggest that core−shell structures are formed in the ordered samples ($f_O \geq 0.07$). The degree of O block crystallinity was determined calorimetrically as reported in Table 1 (see Supporting Information for DSC curves). Transition from the disordered state to the LLP sphere phase is associated with a significant increase in O crystallinity (from 0% in SISO-1 to 30% in SISO-2) consistent with at least partial segregation of the S and O blocks. The amount of crystallinity increases with f_O up to a value of 50 to 64% in the HEX phase region. This level of crystallinity is similar to that reported by Bailey et al. in a series of ISO triblock terpolymers with well-segregated O domains.[14] The possibility of mixed S + O domains also exists at elevated temperatures as the enthalpic penalty between the blocks decreases. Order-order transitions from "three-domain" to "two-domain" structures have been reported in several ABC triblock terpolymer systems.[33−35]

Core−shell structures are favorable due to the block sequence and segment−segment interactions ($\chi_{IO} > \chi_{IS} \cong \chi_{SO}$) present in

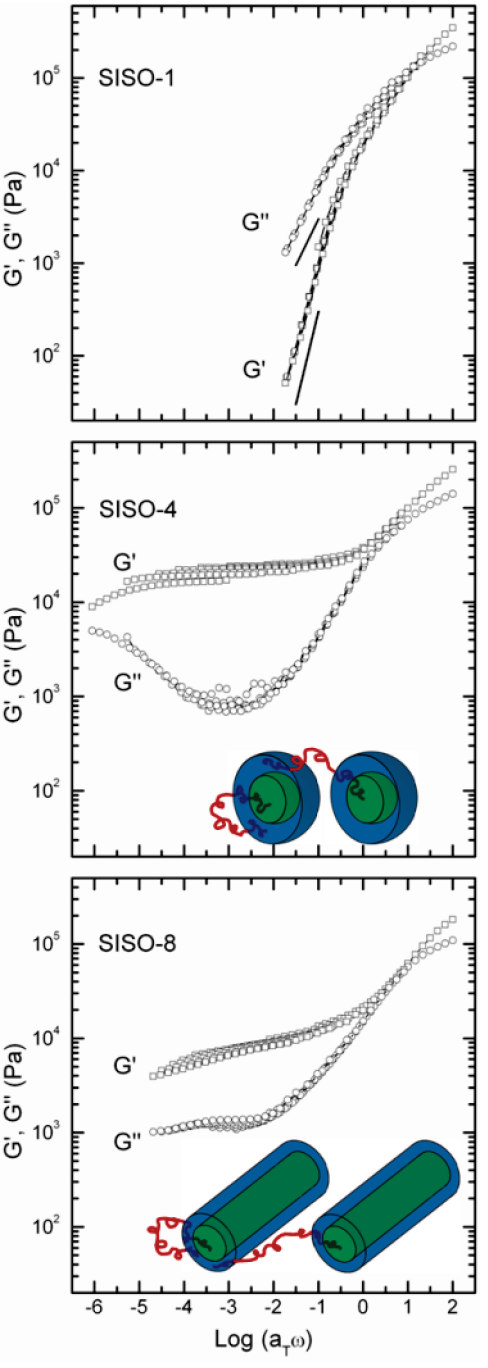

Figure 3. Isothermal frequency sweep data shifted according to time−temperature superposition ($T_{ref} = 80$ °C) for samples possessing the three distinct microstructures discussed in this work. SISO-1 ($80 \leq T \leq 110$ °C) exhibits liquid-like terminal behavior associated with the disordered phase ($G' \sim \omega^2$ and $G'' \sim \omega$). The solid black lines near G' and G'' indicate slopes of two and one, respectively. The data for SISO-4 ($80 \leq T \leq 220$ °C) display a low-frequency plateau in G' is consistent with the spherical microstructure determined on the basis of SAXS and TEM. SISO-8 ($80 \leq T \leq 240$ °C) yielded qualitatively different frequency results with a weak dependence of G' and G'' on ω at low frequencies.

SISO. Addition of a short O chain to the SIS triblock (SISO-1, $f_O = 0.04$) does not disrupt the state of disorder above 80 °C. Increasing the O block length (SISO-2, $f_O = 0.07$) induces microphase separation, driven primarily by unfavorable interactions between the I and O blocks, and to a lesser extent the S and I blocks. Core (O)−shell (S) microstructures are able to utilize S as an insulating barrier between highly unfavorable I/O contacts

while maintaining the chain connectivity dictated by the SISO molecular architecture. Additionally, the two architecturally dissimilar S blocks are incorporated, without discrimination, into the shell of the core−shell morphologies. For samples with lower O content (SISO-2, SISO-3, and SISO-4, $f_O = 0.07-0.09$), the observed core−shell particles are spheres (see illustration in Figure 3). Increasing the O chain length ($f_O = 0.12$ and higher) reduces the O domain curvature driving a transition to core−shell cylinders as depicted in Figure 3. The packing constraints of the asymmetric SISO molecules are satisfied by embedding the minority O within shells of S in a matrix of I. These core−shell phases minimize the chain stretching penalty associated with the S chains that must span the S/O and S/I interfaces (half of the S blocks) while I chains are free to adopt looping and bridging configurations (see Figure 3).

The core−shell morphologies documented in SISO differ dramatically from the equilibrium microstructures identified in ISO triblocks with comparable compositions. An orthorhombic network structure (O^{70}) possessing *Fddd* symmetry was found to be stable over a wide range of O content ($0.13 \leq f_O \leq 0.24$) along the $f_I = f_S$ isopleth. Like the double gyroid morphology, the O^{70} phase is constructed of trivalent connectors, but possesses lower symmetry. Two- and three-domain lamellae phases bracketed the multiply continuous O^{70} region at lower and higher f_O, respectively.[14,16] Changing the molecular architecture from ISO to SISO drives a preference from the hyperbolic interfaces inherent in network morphologies, like O^{70}, to the higher, and zero Gauss, curvature surfaces present in spheres and cylinders.

A core (O)−shell (S) cylinder microstructure is favored even when f_O approaches f_I and f_S, which is the case for SISO-9 ($f_O = 0.30$). A similar inverted cylindrical phase, where a minority component forms the continuous domain, has been identified in SIO,[13] poly(isoprene-*b*-styrene-*b*-dimethylsiloxane),[33] and diblock/triblock copolymer blends.[36] Extensive characterization of the phase behavior of ISO over a wide range of compositions has not yielded similar structures. In the previous examples of inverted cylindrical phases, the segment−segment interaction parameters are asymmetric ($\chi_{BC} > \chi_{AB} \cong \chi_{AC}$), whereas this is not the case for ISO ($\chi_{AC} > \chi_{AB} \cong \chi_{BC}$).

ABAC tetrablocks have the potential to produce ordered morphologies that are remarkably different from the microstructures formed by ABC terpolymers of the same composition. Determining the specific effects of the asymmetric placement of A blocks in the ABAC architecture will require further experimental and theoretical studies. We have shown that SISO has qualitatively different phase behavior compared to ISO at identical compositions and similar segregation strengths. While ISO samples formed a three-dimensional, orthorhombic network microstructure over a wide range of f_O, inverted spherical and cylindrical morphologies were discovered in SISO. An investigation of complementary asymmetric SISO isopleths, where f_I/f_O is varied, is currently underway.

Acknowledgment. This work was supported by the Department of Energy through a subcontract to UT-Battelle (No. 4000041622) and the National Science Foundation through grant DMR- 0704192, and the University of Minnesota Materials Research Science and Engineering Center (MRSEC DMR-0819885). Portions of this work were performed at the DuPont-Northwestern-Dow Collaborative Access Team (DND-CAT) located at Sector 5 of the Advanced Photon Source (APS). DND-CAT is supported by E.I. DuPont de Nemours & Co., the Dow Chemical Company, and the State of Illinois. Use of the APS was supported by the U.S. Department of Energy, Office of Science, Basic Energy Sciences, under contract No. DE-AC02-06CH11357. Parts of this work were carried out in the University of Minnesota I.T. Characterization Facility, which receives partial support from NSF through the NNIN program. We thank Adam J. Meuler for his assistance in synthesizing these materials.

Supporting Information Available: Figures showing heating and cooling DSC curves. This material is available free of charge via the Internet at http://pubs.acs.org.

References and Notes

(1) Lodge, T. P. *Macromol. Chem. Phys.* **2003**, *204*, 265–273.
(2) Takenaka, M.; Wakada, T.; Akasaka, S.; Nishitsuji, S.; Saijo, K.; Shimizu, H.; Kim, M. I.; Hasegawa, H. *Macromolecules* **2007**, *40*, 4399–4402.
(3) Matsen, M. W.; Bates, F. S. *J. Polym. Sci., Part B* **1997**, *35*, 945–952.
(4) Matsen, M. W. *Phys. Rev. Lett.* **2007**, *99*, 148304/1–148304/4.
(5) Mogi, Y.; Kotsuji, H.; Kaneko, Y.; Mori, K.; Matsushita, Y.; Noda, I. *Macromolecules* **1992**, *25*, 5408–5411.
(6) Gido, S. P.; Schwark, D. W.; Thomas, E. L.; do Carmo Goncalves, M. *Macromolecules* **1993**, *26*, 2636–2640.
(7) Mogi, Y.; Nomura, M.; Kotsuji, H.; Ohnishi, K.; Matsushita, Y.; Noda, I. *Macromolecules* **1994**, *27*, 6755–6760.
(8) Stadler, R.; Auschra, C.; Beckmann, J.; Krappe, U.; Voight-Martin, I.; Leibler, L. *Macromolecules* **1995**, *28*, 3080–3097.
(9) Breiner, U.; Krappe, U.; Abetz, V.; Stadler, R. *Macromol. Chem. Phys.* **1997**, *198*, 1051–1083.
(10) Breiner, U.; Krappe, U.; Thomas, E. L.; Stadler, R. *Macromolecules* **1998**, *31*, 135–141.
(11) Brinkmann, S.; Stadler, R.; Thomas, E. L. *Macromolecules* **1998**, *31*, 6566–6572.
(12) Shefelbine, T. A.; Vigild, M. E.; Matsen, M. W.; Hajduk, D. A.; Hillmyer, M. A.; Cussler, E. L.; Bates, F. S. *J. Am. Chem. Soc.* **1999**, *121*, 8457–8465.
(13) Bailey, T. S.; Pham, H. D.; Bates, F. S. *Macromolecules* **2001**, *34*, 6994–7008.
(14) Bailey, T. S.; Hardy, C. M.; Epps, T. H., III; Bates, F. S. *Macromolecules* **2002**, *35*, 7007–7017.
(15) Avgeropoulos, A.; Paraskeva, S.; Hadjichristidis, N.; Thomas, E. L. *Macromolecules* **2002**, *35*, 4030–4035.
(16) Epps, T. H., III; Cochran, E. W.; Bailey, T. S.; Waletzko, R. S.; Hardy, C. M.; Bates, F. S. *Macromolecules* **2004**, *37*, 8325–8341.
(17) Zheng, W.; Wang, Z. *Macromolecules* **1995**, *28*, 7215–7223.
(18) Bluemle, M. J.; Fleury, G.; Lodge, T. P.; Bates, F. S. *Soft Matter* **2009**, *5*, 1587–1590.
(19) Hillmyer, M. A.; Bates, F. S. *Macromolecules* **1996**, *29*, 6994–7002.
(20) Singh, M.; Odusanya, O.; Wilmes, G. M.; Eitouni, H. B.; Gomez, E. D.; Patel, A. J.; Chen, V. L.; Park, M. J.; Fragouli, P.; Iatrou, H.; Hadjichristidis, N.; Cookson, D.; Balsara, N. P. *Macromolecules* **2007**, *40*, 4578–4585.
(21) Chatterjee, J.; Jain, S.; Bates, F. S. *Macromolecules* **2007**, *40*, 2882–2896.
(22) Fetters, L. J.; Lohse, D. J.; Richter, D.; Witten, T. A.; Zirkel, A. *Macromolecules* **1994**, *27*, 4639–4647.
(23) Kinning, D. J.; Thomas, E. L. *Macromolecules* **1984**, *17*, 1712–1718.
(24) Winey, K. I.; Thomas, E. L.; Fetters, L. J. *Macromolecules* **1992**, *25*, 2645–2650.
(25) Schwab, M.; Stuehn, B. *Phys. Rev. Lett.* **1996**, *76*, 924–927.
(26) Adams, J. L.; Quiram, D. J.; Graessley, W. W.; Register, R. A.; Marchand, G. R. *Macromolecules* **1996**, *29*, 2929–2938.
(27) Sakamoto, N.; Hashimoto, T.; Han, C. D.; Kim, D.; Vaidya, N. Y. *Macromolecules* **1997**, *30*, 1621–1632.
(28) Han, C. D.; Vaidya, N. Y.; Kim, D.; Shin, G.; Yamaguchi, D.; Hashimoto, T. *Macromolecules* **2000**, *33*, 3767–3780.
(29) Dormidontova, E. E.; Lodge, T. P. *Macromolecules* **2001**, *34*, 9143–9155.
(30) Wang, X.; Dormidontova, E. E.; Lodge, T. P. *Macromolecules* **2002**, *35*, 9687–9697.
(31) Kossuth, M. B.; Morse, D. C.; Bates, F. S. *J. Rheol.* **1999**, *43*, 167–196.
(32) Cavicchi, K. A.; Lodge, T. P. *J. Polym. Sci., Part B: Polym. Phys.* **2003**, *41*, 715–724.
(33) Hardy, C. M.; Bates, F. S.; Kim, M.; Wignall, G. D. *Macromolecules* **2002**, *35*, 3189–3197.
(34) Neumann, C.; Abetz, V.; Stadler, R. *Polym. Bull.* **1996**, *36*, 43–50.
(35) Hashimoto, T.; Yamauchi, K.; Yamaguchi, D.; Hasegawa, H. *Macromol. Symp.* **2003**, *201*, 65–75.
(36) Goldacker, T.; Abetz, V. *Macromolecules* **1999**, *32*, 5165–5167.